Facile Synthesis of Graphene Nanosheets *via* Fe Reduction of Exfoliated Graphite Oxide

Zhuang-Jun Fan,[†,*] Wang Kai,[†] Jun Yan,[†] Tong Wei,[†] Lin-Jie Zhi,[‡,*] Jing Feng,[†] Yue-ming Ren,[†] Li-Ping Song,[†] and Fei Wei[§,*]

[†]Key Laboratory of Superlight Materials and Surface Technology, Ministry of Education, College of Material Science and Chemical Engineering, Harbin Engineering University, Harbin 150001, China, [‡]National Center for Nanoscience and Technology of China, Zhongguancun, Beiyitiao 11, Beijing 100190, China, and [§]Beijing Key Laboratory of Green Chemical Reaction Engineering and Technology, Department of Chemical Engineering, Tsinghua University, Beijing 100084, China

ABSTRACT The synthesis of graphene nanosheets from graphite oxide typically involves harmful chemical reductants that are undesirable for most practical applications of graphene. Here, we demonstrate a green and facile approach to the synthesis of graphene nanosheets based on Fe reduction of exfoliated graphite oxide, resulting in a substantial removal of oxygen functionalities of the graphite oxide. More interestingly, the resulting graphene nanosheets with residual Fe show a high adsorption capacity of 111.62 mg/g for methylene blue at room temperature, as well as easy magnetic separation from the solution. This approach offers a potential for cost-effective, environmentally friendly, and large-scale production of graphene nanosheets.

KEYWORDS: graphene nanosheets · Fe reduction · adsorption properties

Graphene, a new class of two-dimensional nanomaterial consisting of a single layer of sp^2 network of carbon atoms, has stimulated wide interests in both the experimental and theoretical scientific community due to its extraordinary electrical, mechanical, and thermal properties.[1−4] These unique features offer great promise for many practical applications including nanoelectronics,[5−9] sensors,[10−13] capacitors,[14,15] and composite reinforcement.[15−17] To achieve these outcomes, the challenges of large-scale production of high quality graphene sheets (GNS) must be overcome.[2]

In recent years, graphene has been prepared by several approaches, such as micromechanical exfoliation of graphite,[1] chemical vapor deposition (CVD),[6,18] epitaxial growth,[19,20] and chemical reduction of graphite oxide (GO).[3,21] Although the reduction mechanism remains ambiguous, chemical reduction of GO is one of the established methods to make graphene in large volume. At present, the chemical reduction of GO is usually fulfilled by using hydrazine,[21,22] dimethylhydrazine,[15] hydroquinone[23] or $NaBH_4$[24,25] as the reducing agent. Unfortunately, the use of these poisonous and explosive reducing agents requires great care. Another problem exists where the additional functional groups introduced during chemical reduction by these reducing agents degrade the electrical properties of graphene.[21] Recently, liquid-phase exfoliation of graphite has opened up a facile way to prepare graphene, but the yield has been quite low (~1 wt %).[26] Therefore, green and facile approaches for mass production of high quality GNS have not yet been achieved.

Iron is the most common element and cheapest metal in the earth. It can be naturally used as a reducing agent owing to its mild reductive ability and nontoxic property. To date, investigations into the synthesis of GNS using a Fe reduction route have not been carried out. Here, we report a green and facile approach to prepare GNS *via* employing Fe as a reducing agent (Scheme 1). Apart from being eco-friendly, our process has several advantages such as high yield, low cost, and short-time processing as compared to previous chemical techniques. Furthermore, we found that the adsorption capacity of GNS for methylene blue (MB) was as high as 111.6 mg/g, and that the MB-adsorbed GNS could be easily collected from the solution by an external magnetic field due to the existence of residual Fe during the reduction.

RESULTS AND DISCUSSION

Our method for preparation of GNS is different from most published ones since it avoids the usage of harmful chemical reductants. Briefly, the dispersion of GO in water was first prepared from graphite by a modified Hummers method. Fe powders

*Address correspondence to fanzhj666@163.com, zhilj@nanoctr.cn, weifei@flotu.org.

Received for review September 8, 2010 and accepted November 17, 2010.

Published online December 7, 2010. 10.1021/nn102339t

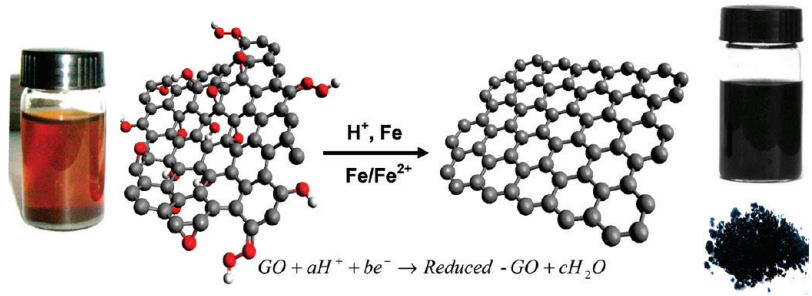

Scheme 1. Illustration of the preparation of GNS based on Fe reduction.

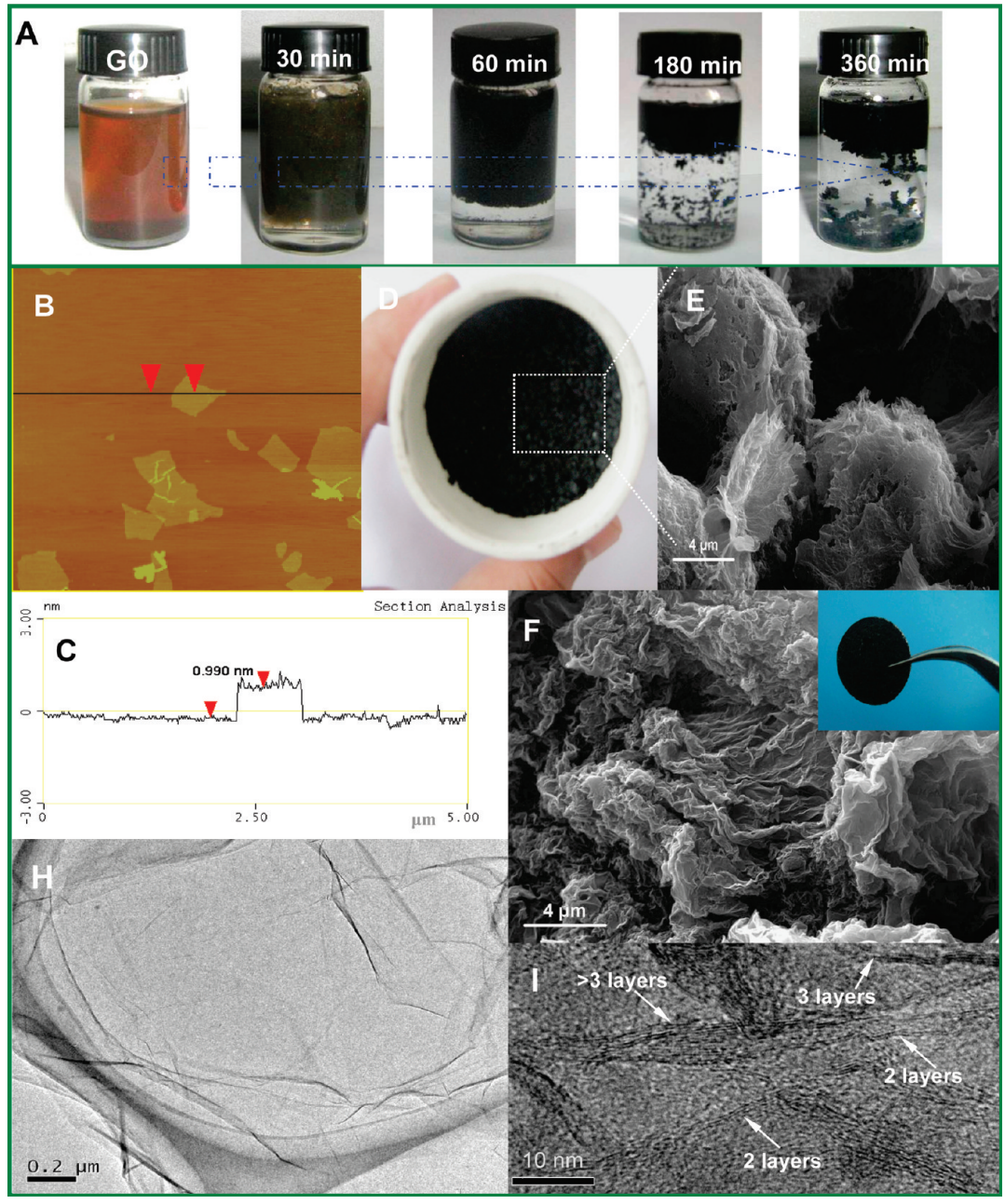

Figure 1. (A) Photographs of aqueous dispersions (0.5 mg/mL) of GO before and after being reduced *via* Fe for different reduction times. (B) AFM image of GO dispersed on mica and (C) corresponding line profile. (D) Photograph and (E) SEM image of reduced GO for 30 min without acid treatment. (F) SEM and (H,I) TEM images of reduced GO for 360 min at different magnifications. The inset of panel F shows the pressed graphene slice.

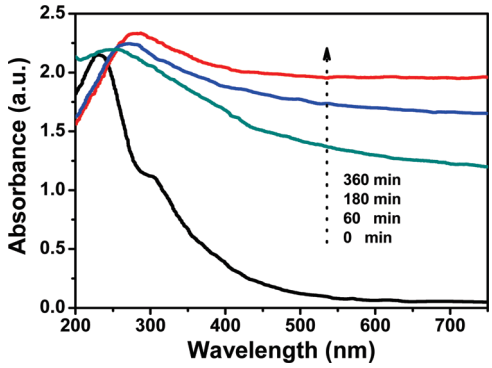

Figure 2. UV−vis absorption spectra showing the change of GO dispersions as a function of reaction time.

and small amount of HCl were then added into GO suspension. The brown color of GO rapidly darkened within 60 min in the presence of both Fe and H^+, as shown in Figure 1A. Due to the hydrophilic nature of the oxygenated graphene layers, GO is easily exfoliated in aqueous media.[27,28] As a result, GO sheets with a thickness of ~1 nm readily form a stable colloidal suspension in water (Figure 1C). After the introduction of H^+, Fe powders react with H^+ to produce Fe^{2+} being adsorbed onto the surface of Fe particles, so that GO sheets with negative charges (−37 mV) are absorbed onto the surface of the positive charged Fe particles to form spherical structures (Figure 1D,E). As a result, the GO sheets closely covering on the surface of Fe particles facilitate the reduction of GO due to the fast electron transport from Fe/Fe^{2+} to GO sheets. The reduction process can be expressed as follows:[29]

$$\text{GO} + a\text{H}^+ + be^- \rightarrow \text{reduced GO} + c\text{H}_2\text{O} \qquad (1)$$

After the reduction of GO for 360 min, microstructure images reveal that the reduced GO material consists of randomly aggregated, thin, crumpled sheets closely associated with each other (Figure 1F,H). Corrugation and scrolling are part of the intrinsic nature of GNS, due to the 2D membrane structure becoming thermodynamically stable *via* bending.[30] Because of scrolling and folding of sheets, it can be observed that the thickness of reduced GO is approximately 1−5 nm and is composed of approximately 2−10 stacked individual monatomic graphene layers, which are clearly shown in the TEM cross section (Figure 1I). This is consistent with the result obtained by the chemical reduction method.[2] By comparison, the reduction rate of GO was very slow in the absence of HCl; even after 2 days the solution was still brown. The introduction of HCl not only dissolves this passive film but also improves the reduction potential of Fe/Fe^{2+}. The reduction progress was first monitored by time-dependent UV−vis spectroscopy as shown in Figure 2. The UV−vis absorption peak of the GO dispersion at 230 nm gradually red shift to 300 nm with increase of reaction time, demonstrating that GO is reduced and the highly conjugated structure like that of graphite is formed gradually during Fe reduction. Little increase in absorption is found after 180 min, indicating completion of most reduction of GO within that period.

Raman scattering is strongly sensitive to the electronic structure and proves to be an essential tool to characterize graphite and graphene materials. In many cases, the Raman spectrum of graphene is characterized by two main features, the *G* mode arising from the first order scattering of the E_{2g} phonon of sp^2 C atoms (usually observed at ~1575 cm^{-1}) and the *D* mode arising from a breathing mode of κ-point photons of A_{1g} symmetry (~1350 cm^{-1}).[31,32] In our study, for the Raman spectrum of GO (Figure 3A), the G band broadens and shifts to 1589 cm^{-1}. Additionally, the D band at 1364 cm^{-1} becomes prominent, indicating a reduction in size of the in-plane sp^2 domains, possibly due to extensive oxidation.[33] The intensity ratio (I_D/I_G) of D band to G band of the GO is about 0.86. Compared with GO, I_D/I_G (1.02) of reduced GO for 30 min increases due to the presence of unrepaired defects that remain after the removal of partial oxygen moieties, and subsequently decreases with the increase of reduction time due to restoration of the sp^2 network during the reduction process.[34] Interestingly, the I_D/I_G (0.32) of GO reduction for 360 min is much lower than most chemical reduction reports, such as $NaBH_4$ (>1),[25] hydrothermal reduction (0.90),[35] hydrazine hydrate (1.63),[36] implying that the Fe

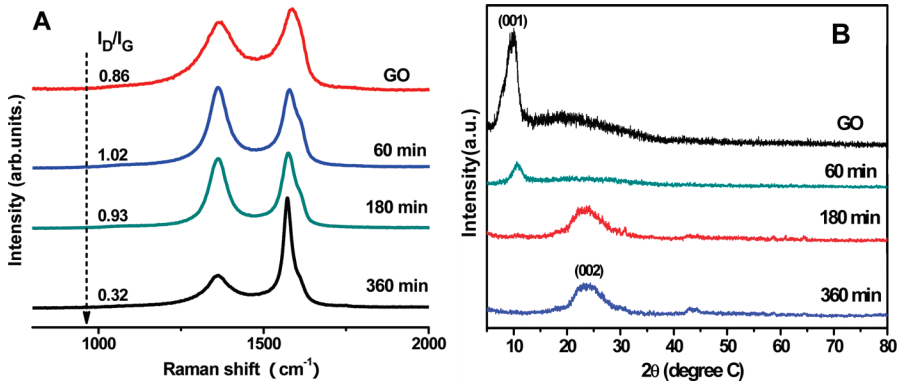

Figure 3. Raman spectra (A) and X-ray diffraction patterns (B) of GO before and after being reduced *via* Fe for different reduction times.

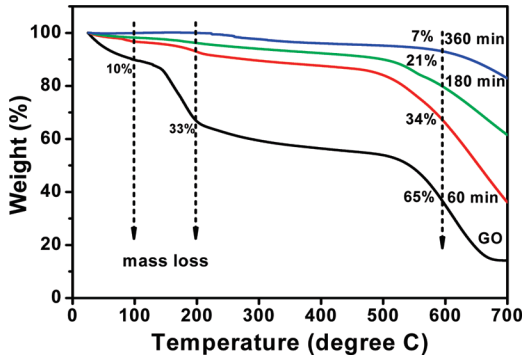

Figure 4. Normalized TGA plots of GO and the obtained GNS.

reduction route is more effective than the other reduction process.

In addition, we further characterized the crystal structure of GNS by XRD. Figure 3B shows the XRD patterns of GO and GNS. Because of the introduction of oxygenated functional groups on carbon sheets, the basal distance of GO obtained from the (001) peak is approximately 8 Å ($2\theta = 10.3°$) which is large compared to that of graphite (0.34 nm). With the increase of the reaction time, the intensity of the (001) peak at 10.3° is significantly reduced, and a small bump appears near 23.2°. This phenomenon is attributed to the removal of some oxygen-containing functional groups. After being reduced for 360 min, the peak at 10.3° disappears com-

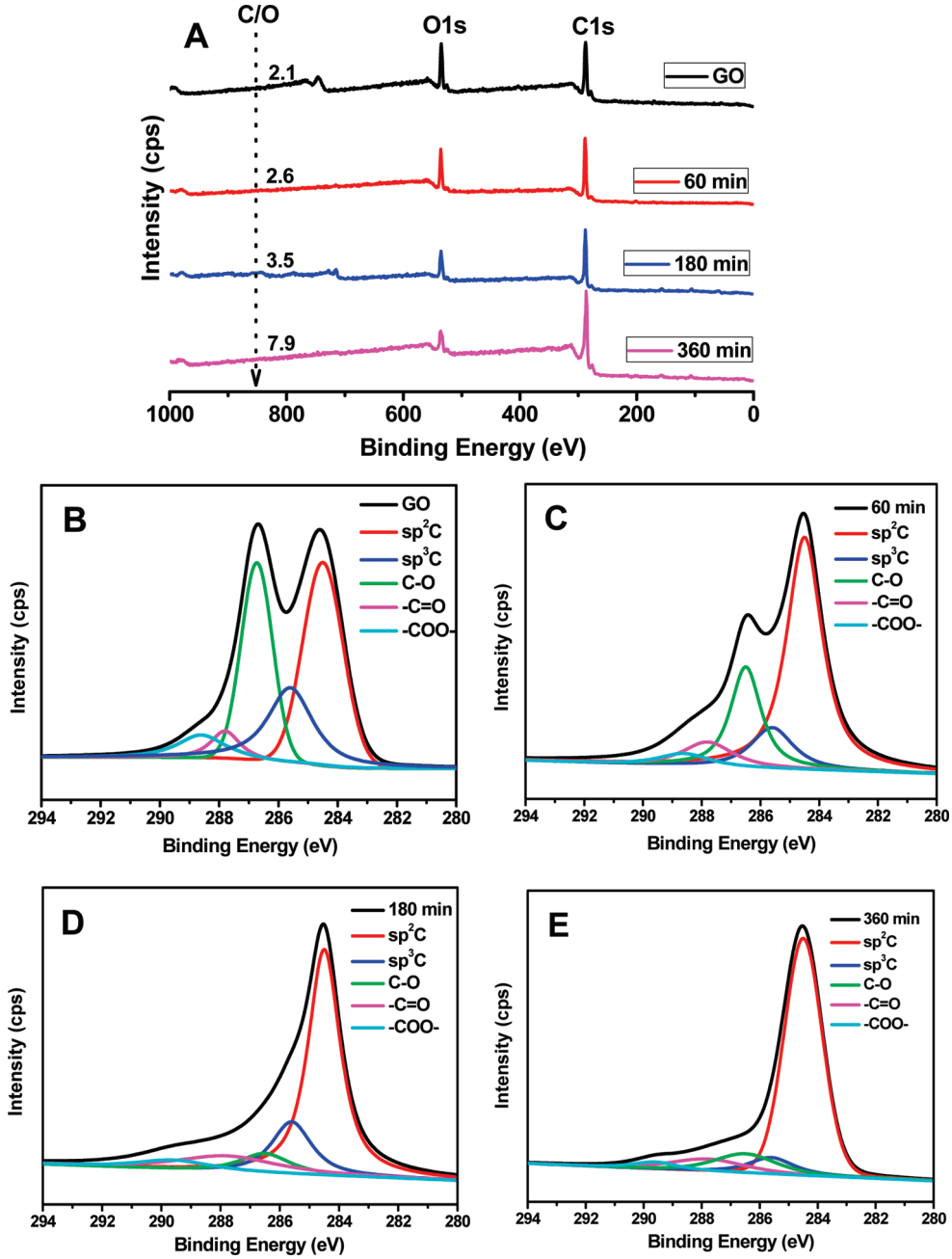

Figure 5. XPS general spectra (A) and curve fit of C1s spectra of GO (B), Fe reduction of GO for 60 (C), 180 (D) and 360 min (E).

TABLE 1. Comparison of Measured Parameters of Graphene Prepared through Different Approaches

materials reduction method	XPS/C:O (atomic ratio)	Raman (I_D/I_G)	TGA at 600 °C (mass loss, %)	electrical properties	ref
GO/$NaBH_4$	5.3	>1	unknown	45 S/m film	25
GO/hydrothermal	5.6	0.90	unknown	unknown	35
GO/solvothermal	6.4	1.16	>20%	0.05 S/m	39
sodium + ethanol				powder	
GO/solvothermal−PC		unknown	>20%	film	40
at 150 °C	8.3			2100 S/m	
at 200 °C	6.8			1800 S/m	
GO/hydroquinone		>2	>50%		41
GO/hydrazine	10.3	>1	>10%	~200 S/m powder	42
GO/prereduction by $NaBH_4$	4.78	1.91	>10%	82.3 S/m	43
heating in H_2SO_4 at 200 °C	8.57	1.00	~10%	1660 S/m	
annealing at 1100 °C in Ar/H_2	>246	0.82	~0%	20200 S/m film	
GO/Fe, at room temperature, 6 h	7.9	0.32	7%	2300 S/m	present work

pletely, and a broad peak at 24.3° appears, indicating the deep reduction of GO and the exfoliation of the layered GNS.[36,37]

Thermal stability of GO and GNS using thermogravimetric analysis (TGA) is shown in Figure 4. For the GO curve, there is a small mass loss (10 wt %) around 100 °C and a major mass loss (33 wt %) around 175 °C due to the loss of adsorbed water and pyrolysis of the labile oxygen-containing functional groups, respectively. Compared to 65 wt % loss at 600 °C for GO, the losses are 34, 21, and 7 wt % after being reduced *via* Fe for 60, 180, and 360 min, respectively, suggesting that the reduced GO exhibits more thermal stability with the increase of reaction time due to the gradual removal of the labile oxygen-containing functional groups.

The degree of GO reduction is described as well *via* the atomic ratio of carbon and oxygen (C/O) obtained by taking the ratio of C1s to O1s peak areas in XPS spectra. As shown in Figure 5A, with increasing reduction time the C/O increases from 2.1 to 7.9. Additionally, from the C 1s XPS spectrum of GO (Figure 5B), five different peaks centered at 284.5, 285.6, 286.7, 287.8, and 288.8 eV are observed, corresponding to sp^2 C, sp^3 C, C−O, −C═O, and −COO− groups, respectively. With the increase of reaction time (Figure 5C−E), the intensities of all C 1s peaks of the carbons binding to oxygen and the peak of sp^3 carbon decrease gradually; these accompany the increase of the peak of sp^2 carbon, revealing that most of the oxygen containing functional groups are removed and the majority of the conjugated graphene networks are restored after the reduction.[38] Table 1 compares those parameters such as C/O atomic ratio, I_D/I_G, mass loss at 600 °C, and electrical conductivity of graphenes prepared through different approaches. Comparison of the available data, the Fe reduction approach described here appears as one of the most attractive routes toward deoxygenation of graphene oxide suspensions.

On the basis of the discussed results, the high quality GNS can be obtained *via* Fe reduction of GO for 360 min after acid treatment. Obviously, there is remaining Fe (less than 1 wt % by XPS analysis) in the graphene sheets without acid treatment. Therefore, the magnetic properties of the resulting GNS at room temperature were characterized using a vibrating sample magnetometer (VSM). As shown in Figure 6, the magnetization hysteresis loop is a S-like curve and the maximum saturation magnetization value reaches 1.66 emu/g. Furthermore, the sample exhibits typical superparamagnetic behavior with no coercivity and remanence, implying that there is no remaining magnetization when the applied magnetic field is removed. Taking advantage of this, we investigated the sample's adsorption ability of MB in aqueous solution. Of interest, the magnetic GNS can be easily separated from the solution by an external magnetic field, and the solution becomes colorless (Figure 6), which favors the reuse of GNS.

The effect of contact time on the resulting GNS adsorption properties from MB solution with a concentration of 12 mg/L is given in Figure 7A, which shows that MB adsorption increases with an increase of contact time. A rapid adsorption increase is observed within 30 min due to the fast surface adsorption of GNS, and a subsequent slow increase indicates that the adsorbed MB slowly migrates from the surface to internal nanosheets. After adsorption for 100 min, a dynamic equilibrium process is established. In addition, the removal efficiency of MB for GNS reaches 97.8% after equilibrium adsorption (Figure 7B).

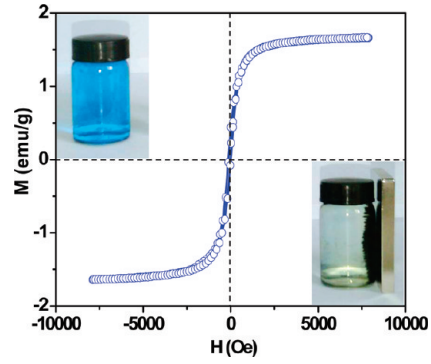

Figure 6. Magnetic hysteresis loops of GNS obtained by Fe reduction for 360 min without acid treatment at room temperature.

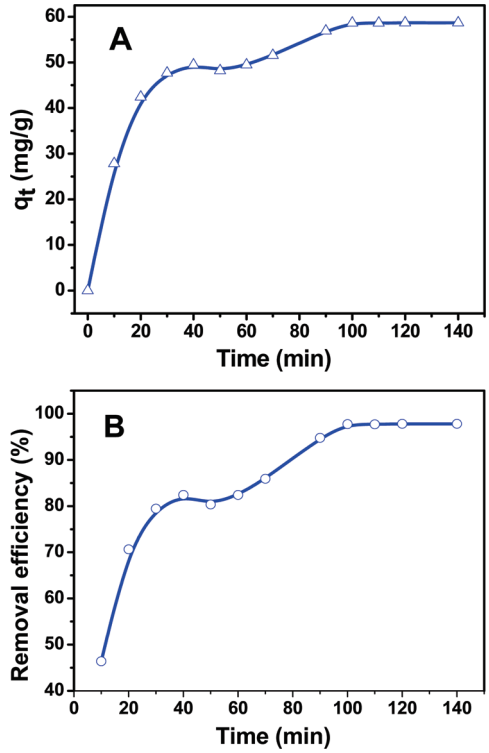

Figure 7. Time-resolved adsorption capacity (A) and the removal efficiency (B) of MB on GNS in a 12 mg/L MB solution at room temperature.

Langmuir model assumes the monolayer coverage of adsorbate over a homogeneous adsorbent surface.[44] The adsorption isotherm is based on the assumption that sorption takes place at specific homogeneous sites within the adsorbent. Once an adsorbate molecule occupies a site, no further adsorption takes place at the same site, with no interaction between adsorbed species. The adsorption isotherm of MB on GNS is shown in Supporting Information, Figure S1. The values of q_e increase with the increase of equilibrium MB concentration. Linear fitting in Langmuir isotherm (Supporting Information, Figure S2) exhibits a high correlation coefficient (R^2) of 0.9965, showing that the adsorption of MB on GNS follows the Langmuir isotherm, with a maximum adsorption capacity q_m of 111.62 mg/g.

To investigate the mechanism of adsorption kinetics, the pseudo-first-order and pseudo-second-order kinetic models were investigated.[45,46] The adsorption kinetic constants and linear regression values are summarized in Table 2. The calculated value of q_e (33.35 mg/g) from the pseudo-first-order kinetic model is dramatically lower than the experimental value (58.64 mg/g). However, the pseudo-second-order kinetic model provides a near-perfect match between the theoretical (59.62 mg/g) and experimental q_e values. In addition, the correlation coefficient (0.9251) given by the first kinetic model (Supporting Information, Figure S3) is lower than that by the pseudo-second-order kinetic model (0.9927), suggesting that an explanation for the adsorption kinetics can be well described by a pseudo-second-order kinetic model, which means that the adsorption rate is dependent on the unoccupied surface of the nanosheets.[44]

TABLE 2. The Kinetics Constants for the Adsorption of MB onto GNS

experimental	q_e (mg/g)	58.64
pseudo-first-order equation	K_1 (min^{-1})	0.1014
	q_{theory} (mg/g)	33.35
	R_1^2	0.9251
pseudo-second-order equation	K_2 ((g/mg)/min)	0.0013
	q_{theory} (mg/g)	59.62
	R_2^2	0.9927

CONCLUSIONS

We have demonstrated that a green and facile approach to the synthesis of GNS *via* Fe reduction results in a substantial removal of oxygen functionalities of the GO. This method avoids the usage of harmful chemical reductants and the introduction of any additional functional groups that are undesirable for most practical applications of graphene. Furthermore, the resulting GNS with remaining Fe shows excellent absorption properties for MB, as well as easy magnetic separation from the solution. The adsorption kinetics can be well described by a pseudo-second-order kinetic model, implying that the adsorption rate depends on the unoccupied surface of nanosheets. Moreover, the adsorption equilibrium data fit the Langmuir isotherm equation well with a maximum adsorption capacity of 111.62 mg/g at room temperature.

EXPERIMENTAL SECTION

Synthesis of GO. GO was synthesized from natural graphite (300 μm, Qingdao Graphite Company) by a modified Hummers method.[47] As-synthesized GO was suspended in water to give a brown dispersion, which was subjected to dialysis to completely remove residual salts and acids. The purified GO were then dispersed in water to make a 0.5 mg/mL suspension. Exfoliation of GO was achieved by ultrasonication using an ultrasonic bath (KQ-600KDE, 600 W).

Reduction of GO *via* Fe. In a typical experiment, 1 g of Fe powder (average particle size: 10 μm, Shanghai CNPC Qifa Powder Material Co., Ltd.) and 20 mL of HCl (35 wt %) were directly added into 100 mL of GO suspension at ambient temperature. The mixture was stirred for 30 min and then maintained for a period of time. After reduction, 15 mL of HCl (35 wt%) was added into the above solution in order to fully remove excess Fe powder. Finally, the resulting GNS was collected with filtration, washed with pure water and ethanol several times, and dried at 100 °C for 12 h in a vacuum oven.

Material Characterization. The crystallographic structures of the materials were determined by a powder X-ray diffraction system (XRD, TTR-III) equipped with Cu Kα radiation (λ = 0.15406 nm). Raman spectra were obtained on a Jobin-Yvon HR800 Raman spectrometer with 457.9 nm wavelength incident laser light. UV−vis detection was carried out on a Shimadzu UV-1601 UV−vis spectrophotometer (Japan). Zetapotential measure-

ments (Zeta Plus, Brookhaven Instruments) were done on the as-dispersed graphene oxide suspension. X-ray photoelectron spectroscopy (XPS) measurements were performed using a PHI 5700 ESCA spectrometer with a monochromated Al Kα radiation ($h\nu$ = 1486.6 eV). All XPS spectra were corrected using the C 1s line at 284.6 eV. Curve fitting and background subtraction were accomplished using Casa XPS version 2.3.13 software. Thermogravimetric analysis (TGA) of sample was performed on a Pyris Diamond TG/DTA thermogravimetric analyzer (Perkin-Elmer Thermal Analysis). The sample was heated under nitrogen atmosphere from room temperature to 700 at 5 °C min^{-1}. Magnetic properties were measured at room temperature with JDM-14D vibrating sample magnetometer (China). The microstructure of the samples was investigated by a scanning electron microscope (SEM, Camscan Mx2600FE), a transition electron microscope (TEM, JEOL JEM2010), and an atomic force microscope (AFM, Nanoscope IIIa). The conductivity of a bulk sample of graphene was taken by pressing the graphene powder into a disk using a 15 mm (diameter) dye under a hydraulic press and measuring the resistance between two points on the sample. The conductivity was calculated using the equation: $R = \rho \times L/A$, where R is resistance, ρ is resistivity, A is the cross-sectional area of the sample in contact with the electrodes, and L is the distance between the electrodes, with the conductivity being the inverse of resistivity.

Adsorption—Desorption Experiments. Batch experiments were conducted in 200 mL Erlenmeyer flasks containing 0.02 g GNS obtained by Fe reduction for 360 min without acid treatment, and with known MB concentrations at room temperature. The flasks were agitated in a vibrator (HY-5, China) at 150 rpm for 3 h to ensure adsorption equilibrium. The adsorbent was separated by a magnet and the MB concentration was analyzed using UV−vis spectrophotometer at 665 nm wavelength. All the experimental data were the averages of duplicate or triplicate determinations. The relative errors of the data were controlled to within 5%.

Adsorption capacity and removal efficiency of MB on different adsorbents were calculated according to the following equations:[48]

$$\text{Removal } \% = \frac{(C_0 - C_e)100}{C_0} \quad (2)$$

$$q_e = \frac{(C_0 - C_e)V}{W} \quad (3)$$

where q_e (mg/g) is the amounts of MB adsorbed onto adsorbent at equilibrium, C_o (mg/L) and C_e (mg/L) are initial and equilibrated MB concentrations, respectively; V (L) is the volume of added solution, and W (g) is the mass of the adsorbent (dry).

To investigate the mechanism of adsorption of MB by adsorbents and the potential rate-controlling steps, kinetic models were applied to evaluate the experimental data. For this purpose Lagergren's pseudo-first-order kinetic model[45] and pseudo-second-order kinetic model[46] were used. The pseudo models are expressed as

$$\log(q_e - q_t) = (\log q_e) - \frac{k_1 t}{2.303} \quad (4)$$

$$\frac{t}{q_t} = \frac{1}{k_2 q_e^2} + \left(\frac{1}{q_e}\right)t \quad (5)$$

where q_t is the amount of Ni (II) removed at the time t (mg/g) and k_1 (min^{-1}) and k_2 ($g \cdot mg^{-1} \cdot min^{-1}$) are the rate constants of the first-order and second-order kinetic equations for adsorption. The data obtained were applied to the Langmuir isotherm using the following linear expression of this model:[44]

$$\left(\frac{C_e}{q_e}\right) = \left(\frac{1}{q_m K_L}\right) + \left(\frac{C_e}{q_m}\right) \quad (6)$$

where q_m is the maximum adsorption capacity of the adsorbent (mg/g), and K_L is the affinity constant (L/mg) related to the adsorption capacity and energy of adsorption, respectively.

Acknowledgment. The authors acknowledge financial support from the National Science Foundation of China (Nos. 51077014, 21003028) and Fundamental Research funds for the Central Universities (HEUCF101006).

Supporting Information Available: Langmuir isotherm plot, linear plots of isotherm, log ($q_e - q_t$) *vs* t and t/q_t *vs* t. This material is available free of charge *via* the Internet at http://pubs.acs.org.

REFERENCES AND NOTES

1. Novoselov, K. S.; Geim, A. K.; Morozov, S. V.; Jiang, D.; Zhang, Y.; Dubonos, S. V.; Grigorieva, I. V.; Firsov, A. A. Electric Field Effect in Atomically Thin Carbon Films. *Science* **2004**, *306*, 666–669.
2. Yoo, E.; Kim, J.; Hosono, E.; Zhou, H.; Kudo, T.; Honma, I. Large Reversible Li Storage of Graphene Nanosheet Families for Use in Rechargeable Lithium Ion Batteries. *Nano Lett.* **2008**, *8*, 2277–2282.
3. Park, S.; Ruoff, R. S. Chemical Methods for the Production of Graphenes. *Nat. Nanotechnol.* **2009**, *4*, 217–224.
4. Geim, A. K. Graphene: Status and Prospects. *Science* **2009**, *324*, 1530–1534.
5. Avouris, P.; Chen, Z.; Perebeinos, V. Carbon-Based Electronics. *Nat. Nanotechnol.* **2007**, *2*, 605–615.
6. Kim, K. S.; Zhao, Y.; Jang, H.; Lee, S. Y.; Kim, J. M.; Kim, K. S.; Ahn, J.-H.; Kim, P.; Choi, J.-Y.; Hong, B. H. Large-Scale Pattern Growth of Graphene Films for Stretchable Transparent Electrodes. *Nature* **2009**, *457*, 706–710.
7. Li, X.; Wang, X.; Zhang, L.; Lee, S.; Dai, H. Chemically Derived, Ultrasmooth Graphene Nanoribbon Semiconductors. *Science* **2008**, *319*, 1229–1232.
8. Gilje, S.; Han, S.; Wang, M.; Wang, K. L.; Kaner, R. B. A Chemical Route to Graphene for Device Applications. *Nano Lett.* **2007**, *7*, 3394–3398.
9. Sui, Y.; Appenzeller, J. Screening and Interlayer Coupling in Multilayer Graphene Field-Effect Transistors. *Nano Lett.* **2009**, *9*, 2973–2977.
10. Schedin, F.; Geim, A. K.; Morozov, S. V.; Hill, E. W.; Blake, P.; Katsnelson, M. I.; Novoselov, K. S. Detection of Individual Gas Molecules Adsorbed on Graphene. *Nat. Mater.* **2007**, *6*, 652–655.
11. Sakhaee-Pour, A.; Ahmadian, M. T.; Vafai, A. Potential Application of Single-Layered Graphene Sheet as Strain Sensor. *Solid State Commun.* **2008**, *147*, 336–340.
12. Zhou, M.; Zhai, Y.; Dong, S. Electrochemical Sensing and Biosensing Platform Based on Chemically Reduced Graphene Oxide. *Anal. Chem.* **2009**, *81*, 5603–5613.
13. Shan, C.; Yang, H.; Song, J.; Han, D.; Ivaska, A.; Niu, L. Direct Electrochemistry of Glucose Oxidase and Biosensing for Glucose Based on Graphene. *Anal. Chem.* **2009**, *81*, 2378–2382.
14. Wang, Y.; Shi, Z.; Huang, Y.; Ma, Y.; Wang, C.; Chen, M.; Chen, Y. Supercapacitor Devices Based on Graphene Materials. *J. Phys. Chem. C* **2009**, *113*, 13103–13107.
15. Stankovich, S.; Dikin, D. A.; Dommett, G. H. B.; Kohlhaas, K. M.; Zimney, E. J.; Stach, E. A.; Piner, R. D.; Nguyen, S. T.; Ruoff, R. S. Graphene-Based Composite Materials. *Nature* **2006**, *442*, 282–286.
16. Watcharotone, S.; Dikin, D. A.; Stankovich, S.; Piner, R.; Jung, I.; Dommett, G. H. B.; Evmenenko, G.; Wu, S.-E.; Chen, S.-F.; Liu, C.-P.; *et al.* Graphene-Silica Composite Thin Films as Transparent Conductors. *Nano Lett.* **2007**, *7*, 1888–1892.
17. Cao, A.; Liu, Z.; Chu, S.; Wu, M.; Ye, Z.; Cai, Z.; Chang, Y.; Wang, S.; Gong, Q.; Liu, Y. A Facile One-Step Method to Produce Graphene−Cds Quantum Dot Nanocomposites as Promising Optoelectronic Materials. *Adv. Mater.* **2010**, *22*, 103–106.
18. Sutter, P. W.; Flege, J.-I.; Sutter, E. A. Epitaxial Graphene on Ruthenium. *Nat. Mater.* **2008**, *7*, 406–411.
19. Berger, C.; Song, Z.; Li, X.; Wu, X.; Brown, N.; Naud, C.; Mayou, D.; Li, T.; Hass, J.; Marchenkov, A. N.; *et al.* Electronic Confinement and Coherence in Patterned Epitaxial Graphene. *Science* **2006**, *312*, 1191–1196.

20. Berger, C.; Song, Z.; Li, T.; Li, X.; Ogbazghi, A. Y.; Feng, R.; Dai, Z.; Marchenkov, A. N.; Conrad, E. H.; First, P. N.; *et al.* Ultrathin Epitaxial Graphite: 2d Electron Gas Properties and a Route toward Graphene-Based Nanoelectronics. *J. Phys. Chem. B* **2004**, *108*, 19912–19916.
21. Stankovich, S.; Dikin, D. A.; Piner, R. D.; Kohlhaas, K. A.; Kleinhammes, A.; Jia, Y.; Wu, Y.; Nguyen, S. T.; Ruoff, R. S. Synthesis of Graphene-Based Nanosheets *via* Chemical Reduction of Exfoliated Graphite Oxide. *Carbon* **2007**, *45*, 1558–1565.
22. Tung, V. C.; Allen, M. J.; Yang, Y.; Kaner, R. B. High-Throughput Solution Processing of Large-Scale Graphene. *Nat. Nanotechnol.* **2009**, *4*, 25–29.
23. Wang, G. X.; Yang, J.; Park, J.; Gou, X. L.; Wang, B.; Liu, H.; Yao, J. Facile Synthesis and Characterization of Graphene Nanosheets. *J. Phys. Chem. C* **2008**, *112*, 8192–8195.
24. Si, Y.; Samulski, E. T. Synthesis of Water Soluble Graphene. *Nano Lett.* **2008**, *8*, 1679–1682.
25. Shin, H. J.; Kim, K. K.; Benayad, A.; Yoon, S. M.; Park, H. K.; Jung, I. S.; Jin, M. H.; Jeong, H. K.; Kim, J. M.; Choi, J. Y.; *et al.* Efficient Reduction of Graphite Gxide by Sodium Borohydride and Its Effect on Electrical Conductance. *Adv. Func. Mater.* **2009**, *19*, 1987–1992.
26. Hernandez, Y.; Nicolosi, V.; Lotya, M.; Blighe, F. M.; Sun, Z. Y.; De, S.; McGovern, I. T.; *et al.* High-yield Production of Graphene by Liquid-phase Exfoliation of Graphite. *Nat. Nanotechnol.* **2008**, *3*, 563–568.
27. Titelman, G. I.; Gelman, V.; Bron, S.; Khalfin, R. L.; Cohen, Y.; Bianco-Peled, H. Characteristics and Microstructure of Aqueous Colloidal Dispersions of Graphite Oxide. *Carbon* **2005**, *43*, 641–649.
28. Szabo, T.; Tombacz, E.; Illes, E.; Dekany, I. Enhanced Acidity and Phdependent Surface Charge Characterization of Successively Oxidized Graphite Oxides. *Carbon* **2006**, *44*, 537–745.
29. Zhou, M.; Wang, Y. L.; Zhai, Y. M.; Zhai, J. F.; Ren, W.; Wang, F. A.; Dong, S. J. Controlled Synthesis of Large-Area and Patterned Electrochemically Reduced Graphene Oxide Films. *Chem.—Eur. J.* **2009**, *15*, 6116–6120.
30. Wang, G.; Shen, X.; Wang, B.; Yao, J.; Park, J. Synthesis and Characterisation of Hydrophilic and Organophilic Graphene Nanosheets. *Carbon* **2009**, *47*, 1359–1364.
31. Tuinstra, F.; Koenig, J. L. Raman Spectrum of Graphite. *J. Chem. Phys.* **1970**, *53*, 1126–1130.
32. Kudin, K. N.; Ozbas, B.; Schniepp, H. C.; Prud'homme, R. K.; Aksay, I. A.; Car, R. Raman Spectra of Graphite Oxide and Functionalized Graphene Sheets. *Nano Lett.* **2007**, *8*, 36–41.
33. Ferrari, A. C.; Robertson, J. Interpretation of Raman Spectra of Disordered and Amorphous Carbon. *Phys. Rev. B* **2000**, *61*, 14095–14107.
34. Gao, W.; Alemany, L. B.; Ci, L.; Ajayan, P. M. New Insights into the Structure and Reduction of Graphite Oxide. *Nat. Chem.* **2009**, *1*, 403–408.
35. Zhou, Y.; Bao, Q. L.; Tang, L. A. L.; Zhong, Y. L.; Loh, K. P. Hydrothermal Dehydration for the "Green" Reduction of Exfoliated Graphene Oxide to Graphene and Demonstration of Tunable Optical Limiting Properties. *Chem. Mater.* **2009**, *21*, 2950–2956.
36. Yan, J.; Fan, Z. J.; Wei, T.; Qian, W. Z.; Zhang, M.; Wei, F. Fast and Reversible Surface Redox Reaction of Graphene-MnO_2 Composites as Supercapacitor Electrodes. *Carbon* **2010**, *48*, 3825–3833.
37. Hassan, H. M. A.; Abdelsayed, V.; Khder, A.; AbouZeid, K. M.; Terner, J.; El-Shall, M. S.; l-Resayes, S. I.; El-Azhary, A. A. Microwave Synthesis of Graphene Sheets Supporting Metal Nanocrystals in Aqueous and Organic Media. *J. Mater. Chem.* **2009**, *19*, 3832–3837.
38. Schniepp, H. C.; Li, J. L.; McAllister, M. J.; Sai, H.; Herrera-Alonso, M.; Adamson, D. H.; Prud'homme, R. K.; Car, R.; Saville, D. A.; Aksay, I. A. Functionalized Single Graphene Sheets Derived from Splitting Graphite Oxide. *J. Phys. Chem. B* **2006**, *110*, 8535–8539.
39. Choucair, M.; Thordarson, P.; Stride, J. A. Gram-Scale Production of Graphene Based on Solvothermal Synthesis and Sonication. *Nat. Nanotechnol.* **2009**, *4*, 30–33.
40. Zhu, Y.; Stoller, M. D.; Cai, W.; Velamakanni, A.; Piner, R. D.; Chen, D.; Ruoff, R. S. Exfoliation of Graphite Oxide in Propylene Carbonate and Thermal Reduction of the Resulting Graphene Oxide Platelets. *ACS Nano* **2010**, *4*, 1227–1233.
41. Wang, G. X.; Yang, J.; Park, J.; Gou, X. L.; Wang, B.; Liu, H.; Yao, J. Facile Synthesis and Characterization of Graphene Nanosheets. *J. Phys. Chem. C* **2008**, *112*, 8192–8195.
42. Stankovich, S.; Dikin, D. A.; Piner, R. D.; Kohlhaas, K. A.; Kleinhammes, A.; Jia, Y.; Wu, Y.; Nguyen, S. T.; Ruoff, R. S. Synthesis of Graphene-Based Nanosheets *via* Chemical Reduction of Exfoliated Graphite Oxide. *Carbon* **2007**, *45*, 1558–1565.
43. Gao, W.; Alemany, L. B.; Ci, L.; Ajayan, P. M. New Insights into the Structure and Reduction of Graphite Oxide. *Nat. Chem.* **2009**, *1*, 403–408.
44. Langmuir, I. The Adsorption of Gases on Plane Surfaces of Glass, Mica, and Platinum. *J. Am. Chem. Soc.* **1918**, *40*, 1361–1403.
45. Lagergren, S.; Svenska, B. K. Zur Theorie Der Sogenannten Adsorption Geloester Stoffe. *Vaternskapsakad Handlingar* **1898**, *24*, 1–39.
46. Cardoso, V. A.; Souza, A. G.; Sartoratto, P. P. C. The Ionic Exchange Process of Cobalt, Nickel and Copper (II) in Alkaline and Acidlayered Titanates. *Colloids Surf. A* **2004**, *248*, 145–149.
47. Hummers, W. S.; Offeman, R. E. Preparation of Graphitic Oxide. *J. Am. Chem. Soc.* **1958**, *80*, 1339.
48. Kumar, P. Y.; King, P.; Prasad, V. Adsorption of Zinc from Aqueous Solution Using Marine Green Algae—*Ulva Fasciata* sp. *Chem. Eng. J.* **2007**, *129*, 161–166.